Geophysical Journal (1989) **96**, 389–399

A model of foreshock occurrence

T. Yamashita* and L. Knopoff
Institute of Geophysics and Planetary Physics, University of California, Los Angeles, CA 90024, USA

Accepted 1988 August 11. Received 1988 August 8; in original form 1987 June 23

SUMMARY

We have constructed a model for the occurrence of foreshocks and foreshock sequences. The foreshocks as well as the main shock are assumed to occur because of the abrupt coalescence of pre-existing cracks. Coalescence occurs if the stress intensity factors at the crack tips exceed a certain critical value. In the sub-critical state each crack undergoes accelerated extension quasi-statically due to stress corrosion, until it reaches the critical state, at which point growth becomes catastrophic.

The rate of foreshock occurrence increases as the time of the main shock approaches and is described by a power law function of time. The exponent in the power law is independent of the distributions of crack sizes, spacings and fracture strengths. This universality implies that foreshock patterns should be useful identifiers for the prediction of the occurrence times of large earthquakes. However, we find that there is considerable diversity in the patterns of energy release. Nevertheless, there is some hope that the magnitudes of large earthquakes can be predicted from the magnitudes of the events in the foreshock sequences if one has *a priori* information describing the distributions of barrier strengths and geometries.

Key words: cracks, earthquake prediction, foreshocks, stress corrosion

1 INTRODUCTION

Case histories that identify foreshocks appear widely in the literature. In a systematic study, Jones & Molnar (1979) examined teleseismically located events before major earthquakes globally from 1914 to 1973, and found that roughly 40 per cent of the main shocks with $M > 7$ were preceded by one or more foreshocks.

While foreshock occurrence has often been suggested as a potential tool for the prediction of large earthquakes, most identifications of foreshocks have been made well after the main shock has occurred. It is extremely difficult to identify a foreshock sequence while it is in progress. A significant exception is the case of the Haicheng earthquake of 1975 in which the identification of foreshocks in progress played a major role in its successful prediction (Raleigh *et al.* 1977). Part of the difficulty with the identification of foreshocks in progress can be attributed to the seemingly great variability of foreshock sequences (Jones and Molnar 1979; Knopoff, Kagan & Knopoff 1982). But more to the point is the difficulty of identifying whether the strongest shock to date is a precursor to an even stronger event or whether it is the strongest of the entire sequence.

In this paper we investigate whether a theoretical model of foreshock occurrence might provide understanding of the nature of foreshock processes and thereby assist in the identification of foreshock sequences in progress. We supplement qualitative theories for foreshock occurrence (e.g. Mogi 1963; Das & Scholz 1981) with quantitative modeling. We shall assume that both the foreshocks and the main shock occur as the result of the sudden coalescence of pre-existing cracks. There is some laboratory evidence that supports this view. Tapponnier & Brace (1976) and Kranz (1979a,b) used evidence from scanning electron microscopy, to show that rock fractures occur due to the coalescence of microcracks. Mogi & Ohnaka (1982) used evidence from the spectra of acoustic emissions prior to the brittle fracture of rocks to show that large cracks are formed in the later stages of deformation as a result of the coalescence of smaller cracks.

To account for the significant time delays between individual foreshocks as well as the main shock, we invoke a stress corrosion cracking mechanism. The relevance of stress corrosion cracking to seismological and geophysical phenomena has been much discussed in recent literature (Anderson & Grew 1977; Das & Scholz 1981; Atkinson 1982; Newman & Knopoff 1982, 1983; Crampin, Evans & Atkinson 1984; Yamashita & Knopoff 1987). Although stress corrosion experiments on rocks are usually restricted to cases of tensile rupture, these experimental results have been applied to theoretical studies of shear fractures in aftershock occurrence by Das & Scholz (1981) and Yamashita & Knopoff (1987). We assume in this paper as well that these results can be applied to the problems of shear fractures.

* Present address: Earthquake Research Institute, University of Tokyo, Tokyo 113, Japan.
Publication No. 3077, Institute of Geophysics and Planetary Physics, University of California, Los Angeles.

We assume that a crack extends catastrophically if the stress intensity factor K exceeds a certain threshold value K_c. In this paper we assume catastrophic fracture is instantaneous, and we bypass the short time-scale dynamical theory of rupture. It is the catastrophic phase that radiates seismic waves and creates the event we identify as an earthquake. Below the critical threshold, the crack is assumed to grow quasi-statically due to stress corrosion.

Kagan & Knopoff (1978) and Jones & Molnar (1979) observed that the temporal rate of increase of foreshock occurrence is well-described by a power law. To model the power law of foreshock occurrence, Jones & Molnar assumed that the fault plane is locked at a number of asperities and considered the problem of the rupture of the full set of asperities; however, they did not discuss explicitly the processes of interaction and coalescence of cracks. In this paper, we explore the physical mechanism of crack interactions in an effort to provide understanding of foreshock processes. In the spirit of the Jones & Molnar model, we describe a foreshock sequence as a hierarchical process of interaction and coalescence of cracks. The time delays between the events will be attributable to stress-corrosion cracking and degradation of the asperities in the fault plane. Our model will yield not only the empirical foreshock power law relationship of Kagan–Knopoff and Jones–Molnar, but also the Gutenberg–Richter relation for the frequency distribution of the moments of foreshocks, at least in the range of small shocks.

2 INTERACTION AMONG COLINEAR PLANE-STRAIN SHEAR CRACKS

Suppose that a large number of small pre-existing cracks are the residue of non-uniform healing of the complex fracture of an earlier earthquake. Suppose further that these pre-existing cracks are 2-D, coplanar and parallel (Fig. 1), and are subjected to plane-strain shear deformation. The projection of the cracks onto an orthogonal plane is that of a line interrupted by gaps. We thus specify the 1-D array of line segments and gaps; these crack sizes and spacings are randomly selected. We specify the distribution functions below.

For the purposes of the analysis below, we need the elastostatic stress-intensity factors at the tips and the seismic moment of each crack. An approximate solution to this problem can be derived if we assume that the suite of cracks influences the stresses at the tips and the moment of one crack in a pairwise manner only; this approximation was made by Chatterjee, Mal & Knopoff (1978) for the study of the elastic properties of composite materials as a multiple scattering process. Under the assumption of pairwise interactions the moment of the kth crack is written in the form

$$M_k = M_k^* + \sum_{i \neq k} (M_{(k,i)} - M_k^*), \tag{1}$$

where M_k^* is the moment of the isolated kth crack and $M_{(k,i)}$ is the moment of the kth crack if we take into account the interaction between the ith and kth crack pair. Similarly, the stress intensity factor of the kth crack is

$$K_k = K_k^* + \sum_{i \neq k} (K_{(k,i)} - K_k^*), \tag{2}$$

with the same notation as in equation (1). Equations (1) and (2) are exact in the case $N = 2$. The solutions for M_k and K_k for the problems of the interaction of two colinear cracks and for the isolated crack are given in Appendix I. The stress intensity factor and the moment are functions of the crack sizes and spacings as well as the stress drop σ_0. The stress drop will be assumed to be constant during the coalescence sequence.

The stress intensity factor and the moment can be obtained exactly for an infinite periodic array of colinear cracks (Koiter 1959; see Appendix II); this solution provides a useful test for the quality of the pairwise assumption. The comparison between the exact solution and that given by the pairwise approximation is shown in Fig. 2. The discrepancy between the two solutions increases as the crack spacing decreases but the error is less than 15 per cent for ratios of crack widths to spacings up to 7:1. We shall assume that the pairwise calculation will be a satisfactory first-order approximation to the crack interaction problem with irregular spacings unless the crack spacing is very small compared with crack size. We can make no statement whether the inclusion of third-order interactions would have given a better approximation for the random colinear case, or indeed in the periodic colinear case for that matter, for the same mean spacing and crack size.

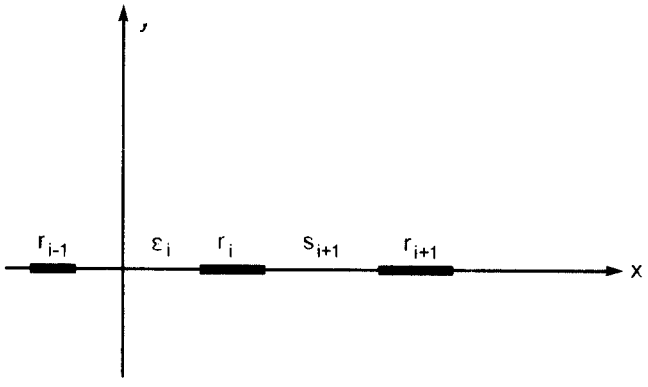

Figure 1. Schematic crack size (r) and barrier spacing (s) distributions.

3 DISTRIBUTION FUNCTIONS

The crack sizes, r, and spacings, s, are assumed to have the power law density distributions,

$$\begin{aligned} p(r) &= C_r r^{-\gamma_0}, \qquad \varepsilon_1 < r < \varepsilon_2 \\ p(s) &= C_s s^{-\gamma_1}, \qquad \eta_1 < s < \eta_2, \end{aligned} \tag{3}$$

where C_r and C_s are appropriate normalization factors, and the εs, ηs and γs are positive constants. The exponents for differential and cumulative distributions γ and D are related by $D = \gamma - 1$.

There is some seismological and experimental evidence to support an assumption of power law distributions: Kagan & Knopoff (1980) and Kagan (1981a,b) showed that the distances between pairs, triplets and quadruplets of earthquake hypocenters have power law distributions. In the case of the distances between pairs, which is in some sense a measure of fracture lengths, the exponent is approximately

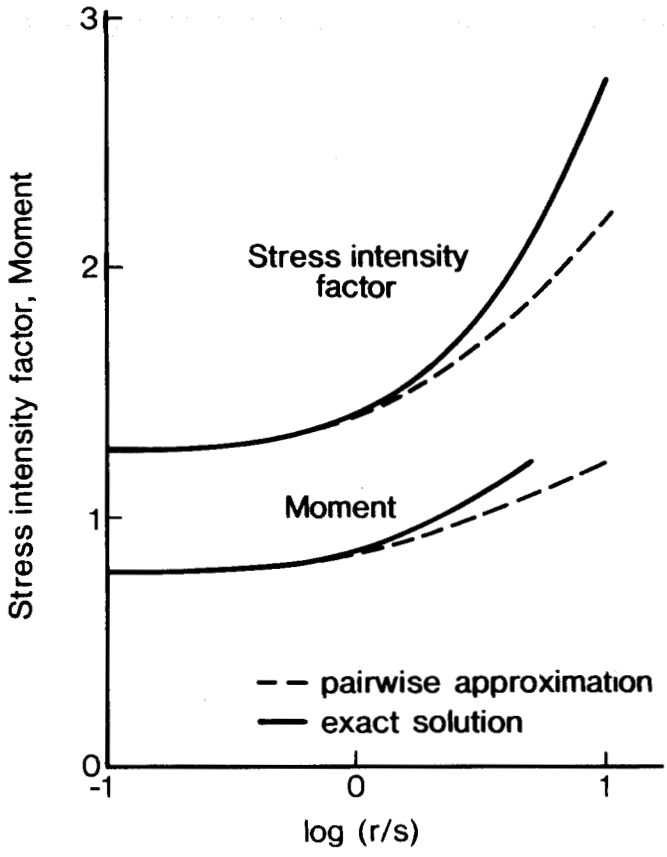

Figure 2. Comparison between the exact and approximate solutions for an infinite periodic array of cracks as a function of crack size to spacing ratio r/s. The approximate solutions are calculated for a case with 200 cracks. The units of non-dimensional stress intensity factor and moment are $K/\sigma_0 L^{1/2}$ and $M/\sigma_0(1-\nu)L^2$, where ν is Poisson's ratio.

$D = 1.0$. On a smaller scale, Segall & Pollard (1983) investigated the frequency distribution of joint lengths in granitic rocks, and showed that it is well-described by a power law distribution with exponents $\gamma = 1.3$ and 1.8 in two cases. Hirata, Satoh & Ito (1987) have found exponents D between 1.25 and 1.75 for distances between acoustic emission foci in brittle fracture experiments.

Aki (1981) has proposed that the fractal dimension for faulting is $\gamma_0 = 3b/d$ where b is the usual slope of the magnitude-log cumulative frequency relation and d is the coefficient in the log moment versus magnitude relation (Wyss & Brune 1968; Thatcher & Hanks 1973). If we take $b = 0.9 \pm 0.1$ and $d = 1.5 \pm 0.3$, then Aki's formula gives $D = 1.8 \pm 0.4$, if the magnitude–frequency law represents a valid long-term average.

Starting with a model of a critical branching process involving elemental earthquakes, Kagan & Knopoff (1981) and Kagan (1982) have shown that the statistical consequences include the power law distribution of fracture sizes, the Omori law of aftershock occurrence and the magnitude–frequency law, among others. While these results do not mandate that the distribution of fracture sizes be a power law, it makes our choice of the form of equation (3) plausible.

Yamashita & Knopoff (1987) found $2 < \gamma < 4$ to be an appropriate range for the distribution of earthquake fault lengths to explain the Omori law of aftershocks. We note that fractal exponents $D > 3$ or $\gamma > 4$ are inappropriate for faults in a 3-D space.

We assume the distributions of the sizes of pre-existing cracks and their spacings are identical to a first-order approximation: $\varepsilon_1 = \eta_1$, $\varepsilon_2 = \eta_2$ and $\gamma_0 = \gamma_1$. In most of our numerical work, the exponent γ will be taken to be 1.2, a value that is a lower bound to the extimates above. To test the influence of variations in the value of γ, we have performed additional experiments with $\gamma = 3.0$, a value that is an upper bound to the experimental estimates we have listed.

The rate of crack growth under the influence of stress corrosion can be described by (Atkinson 1982; Swanson 1984)

$$v = \beta K^n, \tag{4}$$

where v is the crack tip velocity, n is the stress corrosion index and β is a positive coefficient independent of K and n. We assume n is a constant. It has been shown experimentally that n is in the range from 10 to 170; it may be that the lower values of n are favoured for rock materials with pre-existing cracks (Swanson 1984).

The quantity K_c is a critical strength for the onset of catastrophic rupture. At present we have no experimentally derived information that permits us to specify the spatial inhomogeneities of K_c. Therefore, we have made several widely differing *a priori* assumptions regarding the functional nature of the random value of K_c that we assign to the space between each adjacent pair of the initial distribution of cracks (Fig. 3). In models 1, 2 and 3, the value of γ and the range of K_c are all the same; comparison of results for these models displays the effects of different distributions of breaking strengths. Results from numerical experiments using models 1 and 4 allow us to compare the effects of changes in the range of the critical stress intensity factor while keeping the distribution function fixed. Model 5 is the same as model 4 except for the value of the exponent γ.

Qualitatively, the sequence of events is as follows: the lengths of the cracks change with time according to equation (4). The stress intensity factors at each time-step are calculated according to the pairwise approximation of equation (2). As the cracks grow in size, the barriers between them perforce narrow, and as a consequence the stress intensity factors increase with time. Because of the large exponent in (4), the cracks grow at an ever accelerating rate. When the stress intensity factor at any crack-tip becomes equal to its critical value K_c, the crack velocity is instantaneously advanced to an infinite value, and fusion with the adjacent crack takes place. The new stress intensity factors are calculated to see if again any of them exceed their critical values and further fusion takes place if indicated. After a cascade of catastrophic fusion events is completed, the kinematic creep phase resumes. Thus, in the framework of static theory, frequently more than two cracks may coalesce instantaneously if the stress intensity factor at the edge of a first catastrophic fusion exceeds K_c in the next asperity. The change in the seismic moment due to the catastrophic coalescence of cracks can be calculated directly from equation (1). We calculate the moments of the

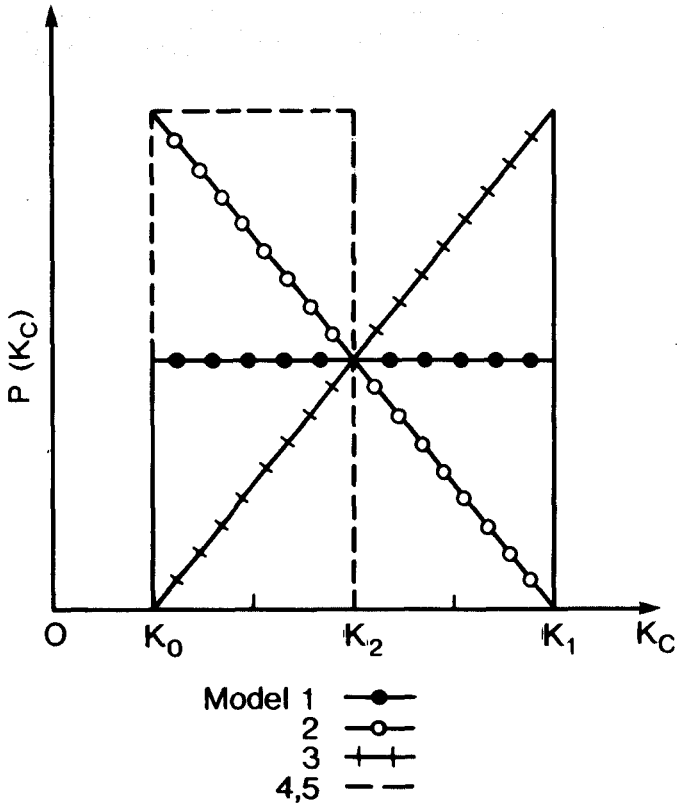

Figure 3. K_c distributions. $K_0 = 0.54$, $K_1 = 2.59$ and $K_2 = 1.57$. The scaling of the stress intensity factor is given in the text. $\gamma = 1.2$ for models 1, 2, 3 and 4; $\gamma = 3.0$ for model 5.

two adjacent cracks, M_k and M_{k+1} at the instant of onset of their catastrophic fusion, as well as the moment M_c of the crack formed by their coalescence. The change in moment due to the coalescence is given by $M_c - M_k - M_{k+1}$ and is the (model) seismic moment. Physically this model can be interpreted to imply that most cracks grow in the pre-fracture creep regime at a microscopic rate, and only accelerate to observable creep and ultimate catastrophic failure in the very last moments of their lifetime.

4 NUMERICAL PROCEDURE

Let the non-dimensional time be $T = \beta\sigma_0^n L^{(n/2)-1} t$ and the non-dimensional crack length be $R = r/L$, where L is an arbitrary unit of length and σ_0 is the stress drop. The ranges of T and R are taken to be arbitrary because the probable range of β is largely unknown; β is highly dependent on temperature, pressure, rock structure, etc. (Atkinson 1984). The units of non-dimensional stress intensity factor and moment are as in Fig. 2. The parameters in equation (3) are assumed to be $\varepsilon_1/L = \eta_1/L = 0.005$ and $\varepsilon_2/L = \eta_2/L = 0.075$. In all computations the stress corrosion index n is fixed at 20. For larger values of this index, crack growth is increasingly more explosive and a more precise numerical treatment is called for, with predictable demands on computer time.

We start by choosing crack sizes, gaps and critical stress intensity factors from the relevant statistical distributions. As indicated, the growth of each crack is calculated numerically from equations (2) and (4) using the distributions of the crack sizes and spacings. One must be careful in the choice of the time-step in the integrations. Since the number of coalescence events per unit time increases, we decrease the size of the time-step as the time of occurrence of the main shock approaches.

To conserve computer time, we have started each numerical experiment with 100 pre-existing cracks. Each numerical experiment is the simulation of one foreshock sequence. However, the few tens of foreshocks formed by binary fusion in these experiments is too small a number for statistical analysis. The average numbers of foreshocks in an individual foreshock sequence are 31, 18, 44, 12 and 32, for models 1–5 respectively. For statistical purposes, we have super-imposed, to a common main shock time, the results of 25 numerical experiments in the cases of models 1, 3 and 5, each with a different set of values of K_c, and 60 experiments in each of the cases of models 2 and 4, to form five different 'summation sequences'. A similar superposition procedure was used by Kagan & Knopoff (1978) and Jones & Molnar (1979) for the statistical analysis of foreshock sequences.

5 FREQUENCY DISTRIBUTION OF FORESHOCK MOMENTS

The frequency–moment curves that result from the numerical simulations are correlated with the difference in range among the models for the strength K_c (Fig. 4). As might have been expected, the upper limit of the frequency–moment distributions depends almost exclusively on the upper limit of size of the distribution of K_c: models with larger strengths have more large earthquakes since these systems can store more potential energy of deformation prior to fracture and hence release more energy in an earthquake. Neither the details of the distribution of K_c or the choice of the exponent γ influence the shape of the frequency–moment curve significantly.

Seismological practice suggests that we compare these results with the Gutenberg–Richter magnitude–frequency law rewritten for seismic moments,

$$\log N(M_0) = \text{const.} + (b/d) \log M_0. \quad (5)$$

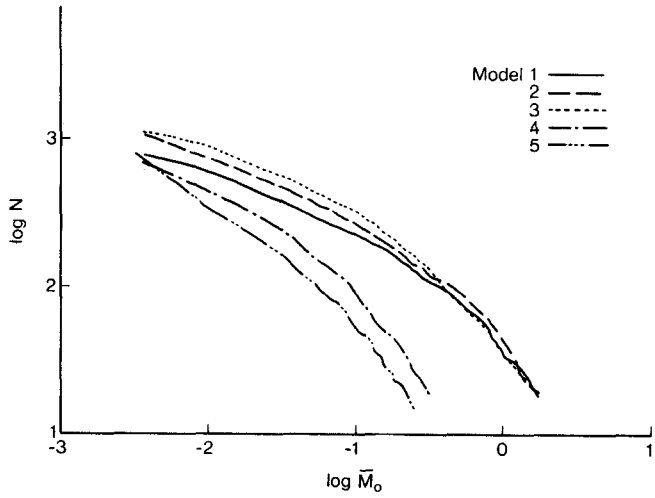

Figure 4. Frequency distribution of foreshock moments.

The slope of our curves is in rough agreement with the expectation from equation (5), although all of the curves in Fig. 4 have a significant downward concavity. The curvature in our moment–frequency relation is also expected to occur in most cases of real earthquake catalogs because of the influence of a maximum magnitude cutoff on the statistical relationships (Kagan & Knopoff 1977, 1984). It is likely that the linear or self-similar range of our frequency law at smaller moments, can be extended significantly by taking larger numbers of cracks initially, either by increasing the length of the array, by changing the lower limit of the distribution, or by going to 2-D faulting. The coefficient in the linear relation b/d, does not depend significantly on the values of γ or the distribution function of K_c, but does depend strongly on the range of K_c, as noted.

6 TEMPORAL VARIATION OF FORESHOCK OCCURRENCE RATE

An example of the temporal variation of the occurrence of shocks arising from the sequence of fusion events in the catastrophic phase is given in Fig. 5 for model 1. We display the number of foreshock events for 40 time-steps before the main shock, for three selected time-scales before the last and main shock. As expected, foreshocks appear more abundantly later in the sequence because most cracks are growing rapidly shortly before the final event; it is the final event that creates a single large crack out of all the others. There is a strong imprint of self-similarity to the sequence, gauged by the similarity of the three histograms, which are successive temporal magnifications by a factor of 10 of the instant before the main shock. Results for the other four models, that involve variations in the distribution functions for the crack sizes or the critical breaking stresses, are startingly similar to those shown in Fig. 5.

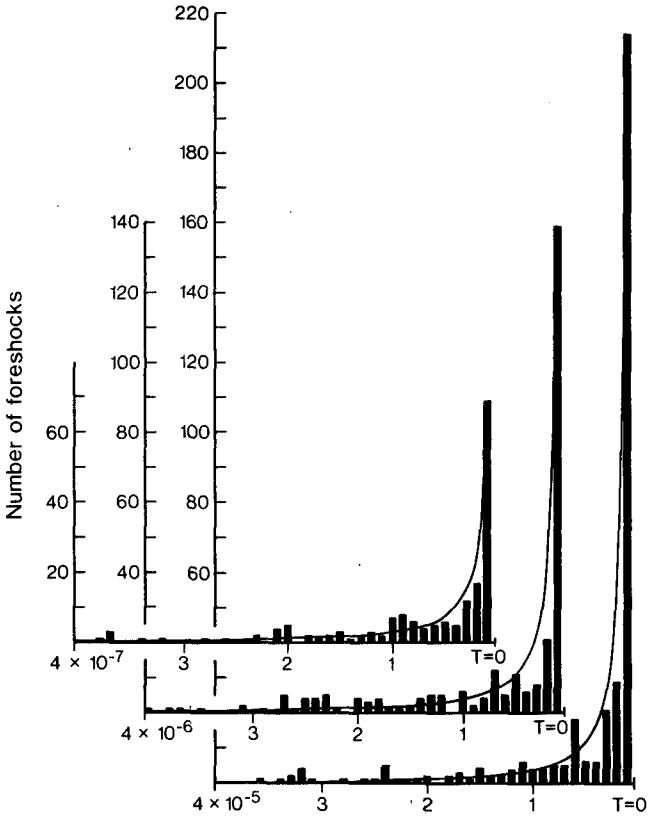

Figure 5. Temporal variation of number of foreshocks in model 1 for three different time-scales before the main shock. The main shock is at $T = 0$. Histograms are averages over 25 simulations.

We seek a fit to the observations of the occurrence of foreshocks with the power law

$$n(T_s) = A(T_s)^{-\alpha}, \tag{6}$$

where $n(T_s)$ is the number of foreshocks per unit time at time T_s before the main shock, and A and α are positive constants (Fig. 6). We estimate the two coefficients by a maximum likelihood procedure (Table 1) and find that α is remarkably independent of the time scale over a broad range of precursor times, varying by not much more than a factor of 2 over 6 orders of magnitude in the scale of times before the main shock. α is similarly independent of γ (compare results from models 4 and 5) as well as the shape of the distribution of K_c.

The values of α are smaller for small strengths, as measured by the upper limit of K_c. Thus equation (6) seems to be a *universal* relation for these simulations of foreshock activity, and is robust relative to broad variations in the properties of fault strengths. This relation, equation (6), is formally similar to the Omori law for aftershocks and to the Omori-like law for foreshocks that has been derived from statistical considerations that are similar to ours; the lower range of our exponents, namely those nearer 1.0, are consistent with the observations of Jones & Molnar and Kagan & Knopoff. For all models, our results show that the exponent is closer to 1.0 in the later stages of the foreshock simulations; this is a time interval before the main shocks that may be more likely to simulate real observations of foreshocks above modern detection thresholds. This suggests that if it were possible to record low-level foreshock sesimicity, that is presumably several orders of magnitude below this level at present, we might be able to observe a change in the value of α as a predictive device. On the other hand lower values of α are observed for models 4 and 5 than with the others; if this were significant, the range of breaking strengths in the earth would be required to be quite narrow. Further numerical experiments are required before such a conclusion would be warranted, but if it should turn out to be the case, then the relation (6) would be valid over a broader interval of time before the main shock. In any case the end result seems to be wholly insensitive to the choice of the exponent γ.

The relation (6) has been applied only to the smoothed summation sequences. In our numerical experiments, an individual foreshock sequence is generally more variable than the smoothed relation (6); we expect that the rate of foreshock occurrence in an individual sequence will become much smoother and much better approximated by equation (6) as the number of initial cracks is increased.

On the other hand, real foreshock sequences are also extremely variable. We can expect that foreshock sequences of actual earthquakes will also be much better approximated by equation (6) if the threshold value of the detection magnitude can be lowered in comparison with most present-day thresholds and if it becomes routinely possible that near-field observations can be made. Jones & Molnar

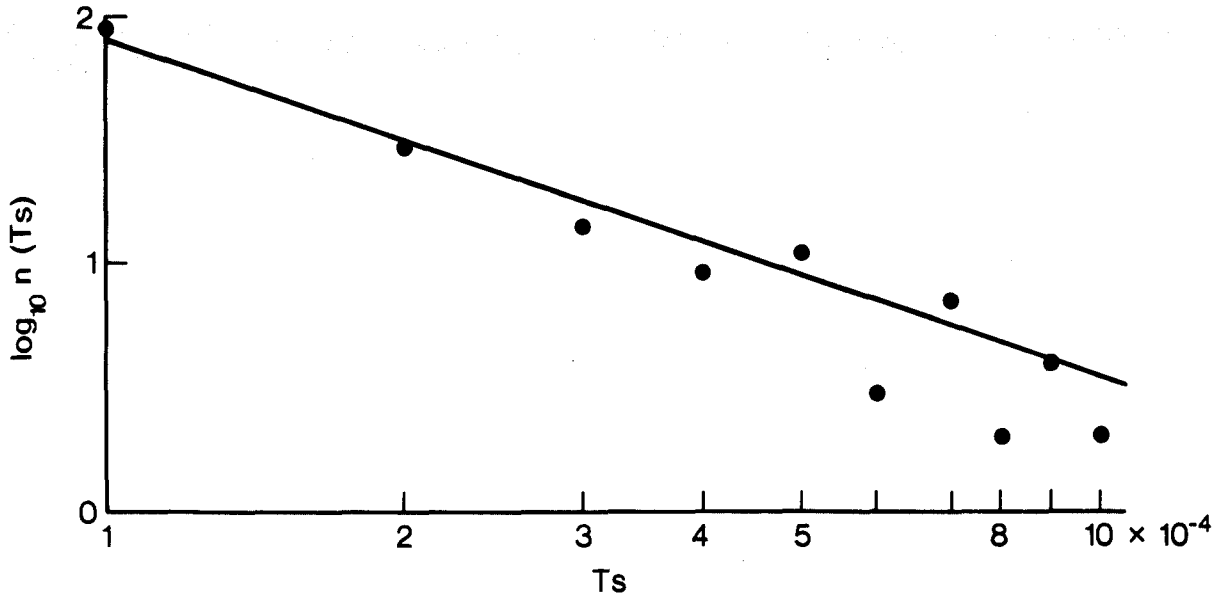

Figure 6. Temporal variation of the number of foreshocks for model 5 at several times T_s before the main shock. The line is the least-squares fit. The main shock is far to the left of the graph. $\Delta T = 10^{-4}$.

(1979) showed that many events are preceded by foreshocks that are not teleseismically determined. In an outstanding example, none of the more than 500 foreshocks of the 1975 Haicheng earthquake was teleseismically located (Wu *et al.* 1976). Near-field observations with low magnitude threshold are especially necessary to identify the early parts of foreshock sequences which are rich in small events. At the present time many main events are preceded by only a small number of detectable foreshocks.

In theory, the application of equation (6) to an individual foreshock sequence will require that curve-fitting be repeated at each time-step, to improve the degree of reliability of prediction of the time of occurrence of the main shock as the event approaches; this is not practical in most cases due to the present paucity of foreshock events in individual earthquake sequences. In fact curve-fitting of any type for most real foreshock sequences is probably unjustified.

Foreshock activity as described by equation (6) has been observed for a few individual foreshock sequences. Using a microearthquake detection network Ishida & Ohtake (1984) found that foreshocks before the small Shizuoka–Seibu earthquake of 1981 ($M = 2.8$) are well described by equation (6). Papazachos (1973) investigated the temporal variation of foreshock activity of three reservoir-associated earthquakes and found that all three foreshock sequences are well described by equation (6) with exponent α ranging from 1.5 to 2.6.

7 TEMPORAL RATE OF SEISMIC ENERGY RELEASE

Since the radiated seismic energy is approximately proportional to the seismic moment, the seismic energy radiated in a given time-step can be calculated by summing the moments of all of the events in the step. Hence we can trace the temporal evolution of the history of seismic energy release, as well as determine its absolute level (Fig. 7). The average value of energy in the main shock is also indicated. We also show variations of the seismic energy radiated in epochs near and far from the occurrence of the main shock. The seismic energy increases rapidly as the main shock is

Table 1. Estimates of α.

ΔT	1.0×10^{-2}	10^{-3}	10^{-4}	10^{-5}	10^{-6}	10^{-7}	10^{-8}
Model 1	2.53	2.34	2.09	1.96	1.69	1.42	1.28
	(0.05)	(0.05)	(0.06)	(0.07)	(0.07)	(0.08)	(0.09)
Model 2	2.23	1.96	1.86	1.59	1.52	1.37	1.40
	(0.05)	(0.05)	(0.06)	(0.06)	(0.07)	(0.08)	(0.10)
Model 3	2.73	2.48	2.21	1.96	1.76	1.48	1.16
	(0.03)	(0.04)	(0.05)	(0.05)	(0.06)	(0.06)	(0.06)
Model 4	1.76	1.57	1.39	1.33			
	(0.07)	(0.08)	(0.09)	(0.10)			
Model 5	1.70	1.55	1.34	1.02	1.00		
	(0.07)	(0.08)	(0.08)	(0.08)	(0.12)		

ΔT is the time increment from the function given in equation (6). Numbers in parentheses are twice the standard deviations of the estimates.

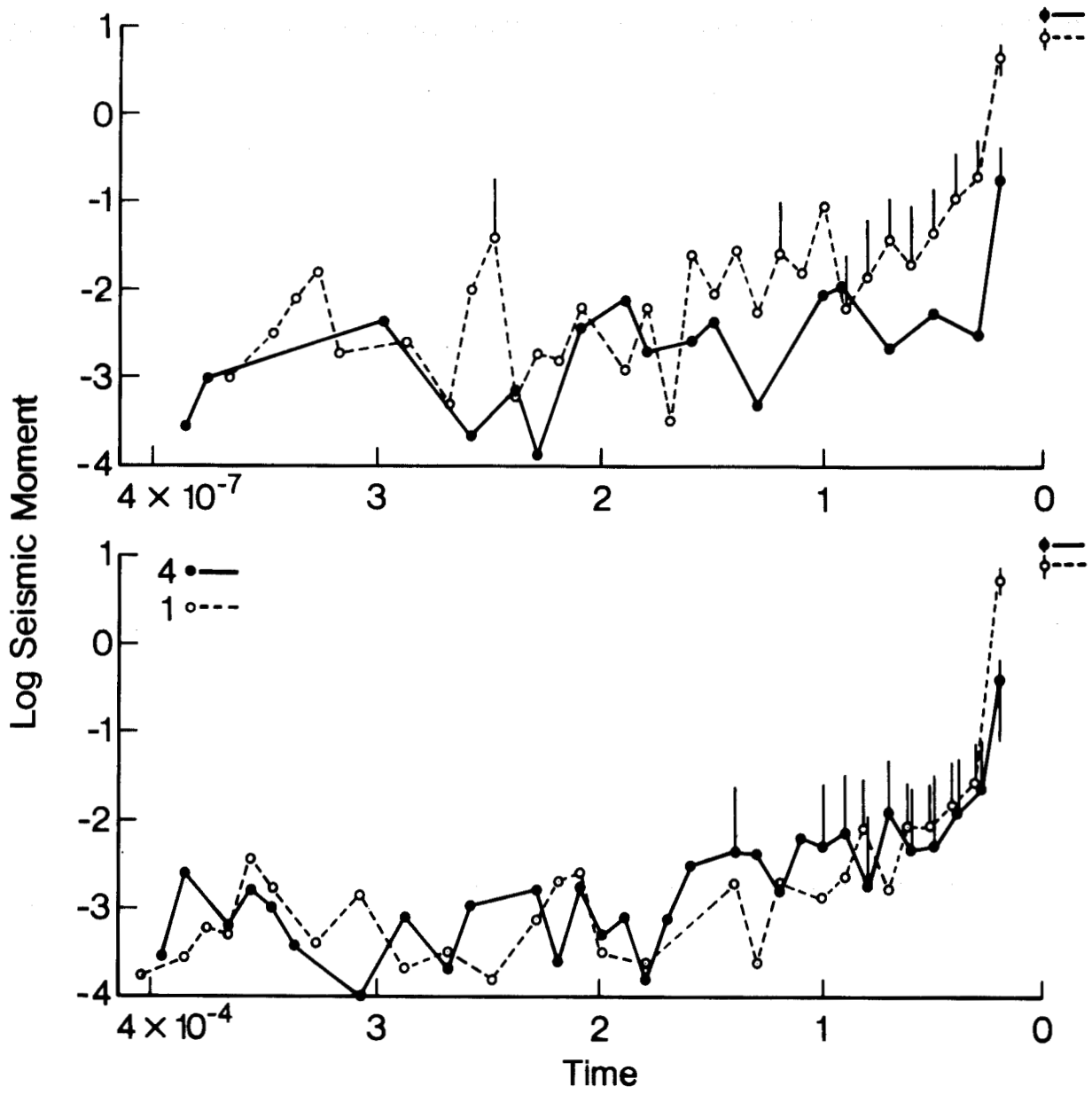

Figure 7. Temporal variation of moment (or seismic energy) released for two models (1 and 4) with different ranges of K_c. The symbols denote the moment in a given time step of the foreshock sequences averaged over all the simulations. The horizontal bars at the upper right of each diagram denote the moment of the main shock. The error bars indicate one standard deviation and are shown only for those cases for which at least five events occurred in a given time step in all of the numerical experiments. The one-sided error bars are for the cases for which the distributions were sufficiently skewed or bimodal that the standard deviations are greater than the average moments and indicate only the positive value. Upper diagram is a magnification of the last instants of the lower diagram.

approached, both because of the increase in the occurrence rate of foreshocks (Fig. 6), and the generation of larger events later in the sequence. However, the general impression given by Fig. 7 is one of great variability in seismic energy release, even after averaging over many simulations. The temporal relationship for the energy release in the other models show similar erratic behaviour.

With regard to the effect of different ranges of K_c on the foreshock energy history, all other parameters in the models being the same, we find that the model with the larger range of K_c generally has larger foreshocks close to the time of the main shock, as expected; this is, of course, the model that can store greater amounts of potential energy of deformation. Although the two models differ by only about 60 per cent in the upper limits of K_c, the amount of energy released in foreshocks in the last 10^{-7} or so before the main shock differ by about an order of magnitude.

The model with the larger range of K_c also releases more seismic energy at times more remote from the main shock, but the behaviour in this remote epoch is so irregular that it is clear that even the 25 or 60 repetitions of the experiment were insufficient to provide enough smoothing to draw a clear-cut conclusion. The early part of the temporal epoch seems to be of little value as a diagnostic because of the

extremely erratic character of individual sequences, perhaps due to the small number of cracks in the initial model.

We find that, on the average, the main shocks for the model with the smaller range of K_c, model 4, are stronger than those of the model with the larger range, model 1, even though the energies of the last and largest foreshocks have the inverse relationship. It is possible that the system with the larger foreshocks had depleted a greater part of the available budget for energy release than the model with smaller foreshocks. This suggests that the size of the future main shock may be anti-correlated with the size of the strongest foreshocks for a given volume of fault system, all other conditions being equal. In general, model 4, which has the smallest range of K_c and the smaller value of the two values of γ, has the largest gap of energy/moment between the main shock and the largest of its foreshocks.

We do not find any noticeable dependence of the aftershock moment series on the choice of the exponent γ, all other parameters being fixed (models 4 and 5). Nevertheless, the energies of the main shocks are very different in the two cases of models 4 and 5, being on the average about an order of magnitude larger in the cases of models with smaller values of γ. We may assume that the association of the larger main shock with the smaller value of γ is due to the fact that smaller values of γ imply larger cracks and spacings, and hence that the seismic energy is derived from a larger volume.

The relationships between the rates of foreshock release and the detailed properties of the statistical models for K_c are unclear; the rates of energy release in foreshocks are overwhelmingly erratic; we cannot state with assurance that the distributions with the higher mean values of K_c will have the higher rates of energy release in foreshocks. Nor can we discern differences in the energy released in the main shocks among the three statistical distributions. Statistical fluctuations in the foreshock sequences are so large that it is not possible to resolve differences among the three statistical models, and probably these differences are not going to be particularly important in real sequences.

8 CONCLUSIONS

From numerical experiments for foreshock occurrence, that make use of a stress corrosion model of sub-critical growth of a power law distribution of sizes and spacings, we have reproduced the usual magnitude–frequency law, modified to take maximum-magnitude effects into account. This suggests that our assumptions are not unrealistic. The b-value changes as the foreshock process evolves: large events become more abundant as the time of the main shock approaches. The latter result suggests that the development of a foreshock sequence can be monitored if enough foreshocks can be observed; this conclusion places stringent demands on the sensitivity of the seismographic network.

The temporal rate of foreshock occurrence is described by a power law function whose exponent does not depend significantly on the choice of parameters. This result implies that the temporal rate of foreshock occurrence is describable by a universal relation similar to the Omori law of aftershock activity. Such a universal relation would imply that the time of the main shock is predictable possibly by careful monitoring of foreshock activity. Unfortunately there is significant temporal diversity and variability in the foreshock sequences as well as in the differences between foreshock and main shock energies. This result is consistent with the seismological observations that there is no perceptible relationship between the size of a main shock and its largest foreshock (Jones & Molnar 1979; von Seggern *et al.* 1981) and that the occurrence of a large number of foreshocks does not necessarily mean that a large main shock will follow.

However, we take a more optimistic point of view. We assume that the magnitude of the mainshock *might* be predicted from the foreshock evidence, *if* information regarding the distribution of the range of the strengths of the barriers, and the exponent in the local fault-length distribution γ, were available from independent information. Perhaps the greatest hope in this direction is to search for empirical information about magnitude differences between the largest foreshock and the main shock for many instances of such pairs for a given region; however, this approach requires that analysis be made of seismic histories of lengths that are not available in most active regions of the world. Perhaps an alternative approach to this problem would be to assume that the range of K_c and the size of γ are universals and hence that these ratios are also universals; we have no evidence to suggest that this assumption is tenable.

REFERENCES

Aki, K., 1981. A probabilistic synthesis of precursory phenomena, in *Earthquake Prediction*, vol. 4, eds Simpson, D. W. & Richards, P. G. American Geophysical Union, Maurice Ewing Series.

Anderson, O. L. & Grew, P. C., 1977. Stress corrosion theory of crack propagation with applications to geophysics, *Rev. Geophys. Space Phys.*, **15,** 77–104.

Atkinson, B. K., 1982. Subcritical crack propagation in rocks: theory, experimental results and applications, *J. struct. Geol.*, **4,** 41–56.

Atkinson, B. K., 1984. Subcritical crack growth in geological materials, *J. geophys. Res.*, **89,** 4077–4114.

Chatterjee, A. K., Mal, A. K. & Knopoff, L., 1978. Elastic moduli of two-component systems, *J. geophys. Res.*, **83,** 1785–1792.

Crampin, S., Evans, R. & Atkinson, B. K., 1984. Earthquake prediction: A new physical basis, *Geophys. J. R. astr. Soc.*, **76,** 147–156.

Das, S. & Scholz, C. H., 1981. Theory of time-dependent rupture in the earth, *J. geophys. Res.*, **86,** 6039–6051.

Hirata, T., Satoh, T. & Ito, K., 1987. Fractal structure of spatial distribution of microfracturing in rock, *Geophys. J. R. astr. Soc.*, **90,** 369–374.

Ishida, M. & Ohtake, M., 1984. Seismicity and waveforms of the microearthquakes before and after the Shizuoka-Seibu earthquake, central Japan, *Bull. seism. Soc. Am.*, **74,** 605–620.

Jones, L. M. & Molnar, P., 1979. Some characteristics of foreshocks and their possible relationship to earthquake prediction and premonitory slip on faults, *J. geophys. Res.*, **84,** 3596–3608.

Kagan, Y. Y., 1981a. Spatial distribution of earthquakes: the three-point moment function, *Geophys. J. R. astr. Soc.*, **67,** 976–717.

Kagan, Y. Y., 1981b. Spatial distribution of earthquakes: the four-point moment function, *Geophys. J. R. astr. Soc.*, **67,** 719–733.

Kagan, Y. Y., 1982. Stochastic model of earthquake fault geometry, *Geophys. J. R. astr. Soc.*, **71,** 659–691.

Kagan, Y. Y. & Knopoff, L., 1978. Statistical study of the occurrence of shallow earthquakes, *Geophys. J. R. astr. Soc.*, **55,** 67–86.

Kagan, Y. Y. & Knopoff, L., 1980. Spatial distribution of earthquakes: the two-point correlation function, *Geophys. J. R. astr. Soc.*, **62,** 303–320.
Kagan, Y. Y. & Knopoff, L., 1981. Stochastic synthesis of earthquake catalogs, *J. geophys. Res.*, **86,** 2853–2862.
Kagan, Y. Y. & Knopoff, L., 1984. A stochastic model of earthquake occurrence, *Proc. 8th Int. Conf. Earthquake Engineering*, **1,** 295–302.
Knopoff, L. & Kagan, Y., 1977. Analysis of the theory of extremes as applied to earthquake problems, *J. geophys. Res.*, **82,** 5647–5657.
Knopoff, L., Kagan, Y. Y. & Knopoff, R., 1982. *b*-Values for foreshocks and aftershocks in real and simulated earthquake sequences, *Bull. seism. Soc. Am.*, **72,** 1663–1676.
Koiter, W. T., 1959. An infinite row of colinear cracks in an infinite elastic sheet, *Ingenieur-Archiv.*, **28,** 168–172.
Kranz, R. L., 1979a. Crack growth and development during creep of Barre granite, *Int. J. Rock Mech. Min. Sci. Geomech. Abstr.*, **16,** 23–35.
Kranz, R. L., 1979b. Crack-crack and crack-pore interactions in stressed granite, *Int. J. Rock Mech. Min. Sci. geomech. Abstr.*, **16,** 37–47.
Mogi, K., 1963. Some discussions on aftershocks, foreshocks and earthquake swarm—the fracture of a semi-infinite body caused by an inner stress origin and its relation to the earthquake phenomena (third paper), *Bull. earthq. Res. Inst.*, **41,** 615–658.
Mogi, K. & Ohnaka, M., 1982. Foreshock characteristics of acoustic emission in rocks under uniaxial compression and its relation to the fracture process to failure, *J. geophys. Res.*, **87,** 3873–3884.
Muskhelishvili, N. I., 1953. *Some Basic Problems of the Mathematical Theory of Elasticity*, Noordhoff, Groningen.
Newman, W. I. & Knopoff, L., 1982. Crack fusion dynamics: a model for large earthquakes, *Geophys. Res. Lett.*, **9,** 735–738.
Newman, W. I. & Knopoff, L., 1983. A model for repetitive cycles of large earthquakes, *Geophys. Res. Lett.*, **10,** 305–308.
Papazachos, B. C., 1973. The time distribution of the reservoir-associated foreshocks and its importance to the prediction of the principal shock, *Bull. seism. Soc. Am.*, **63,** 1973–1978.
Raleigh, B., Bennett, G., Craig, H., Hanks, T., Molnar, P., Nur, A., Savage, J., Scholz, C., Turner, R., and Wu, F., 1977. Prediction of the Haicheng earthquake, *Eos, Trans. Am. geophys. Un.* **58,** 236–272.
Segall, P. & Pollard, D. D., 1983. Joint formation in granitic rock of the Sierra Nevada, *Bull. geol. Soc. Am.*, **94,** 563–575.
Swanson, P. L., 1984. Subcritical crack growth and other time- and environment-dependent behavior in crustal rocks, *J. geophys. Res.*, **89,** 4137–4152.
Tapponnier, P. & Brace, W. F., 1976. Development of stress-induced microcracks in Westerly granite, *Int. J. Rock Mech. Min. Sci. geomech. Abstr.*, **13,** 103–112.
Thatcher, W. R. & Hanks, T., 1973. Source parameters of southern California earthquakes, *J. geophys. Res.*, **78,** 8547–8576.
von Seggern, D., Alexander, S. S. & Baag, C.-E., 1981. Seismicity parameters preceding moderate to large earthquakes, *J. geophys. Res.*, **86,** 9325–9351.
Wu, K., Yue, M., Wu, H., Cao, X., Chen, H., Huang, W., Tian, K. and Lu, S., 1976. Certain characteristics of Haicheng earthquake ($M = 7.3$) sequence. *Acta Geophys. Sinica*, **19,** 109–117.
Wyss, M. & Brune, J. N., 1968. Seismic moment, stress, and source dimensions for earthquakes in the California–Nevada region, *J. geophys. Res.*, **73,** 4681–4694.
Yamashita, T. & Knopoff, L., 1987. Models of aftershock occurrence, *Geophys. J. R. astr. Soc.*, **91,** 13–26.

APPENDIX I

Stress intensity factors and moments of an isolated crack and two colinear cracks

The stress and displacement components may be expressed as functions of the complex variable z and its complex conjugate $\bar{z}$ (Muskhelishvili 1953):

$$P_{xx} + p_{yy} = 4 \operatorname{Re} \Phi(z),$$
$$p_{yy} - p_{xx} + 2ip_{xy} = 2(\bar{z}\Phi'(z) + \Psi(z)), \tag{A1}$$
$$2\mu(u_x + iu_y) = \kappa\phi(z) - z\bar{\phi}'(z) - \bar{\psi}(z),$$

where $\Phi(z) = \phi'(z)$, $\Psi(z) = \psi'(z)$, $\kappa = 3 - 4\nu$, and μ is the rigidity and ν is Poisson's ratio.

(1) *An isolated crack*

Let the crack be located on the segment of the x-axis, $-a < x < a$, in the infinite $x - y$ plane. We write (Muskhelishvili 1953, p. 498)

$$\Phi(z) = \Omega(z) = -i\sigma_0(z - (z^2 - a^2)^{\frac{1}{2}})/2(z^2 - a^2)^{\frac{1}{2}}, \tag{A2}$$

where $\Omega(z) = \bar{\Phi}'(z) + z\bar{\Phi}'(z) + \bar{\Psi}(z)$, $\bar{\Phi}(z) = \Phi(z)$ and $\bar{\Psi}(z) = \Psi(z)$. Hence the stress intensity factor K and the displacement discontinuity $\Delta u_x(x)$ across the crack are

$$K = \lim (2\pi(x - a))^{1/2} p_{xy}(x, y = 0) = \sigma_0(\pi a)^{1/2}, \tag{A3}$$
$$\Delta u_x(x) = 2(1 - \nu)\sigma_0(a^2 - x^2)^{1/2}/\mu.$$

The moment is therefore,

$$M_0 = \mu \int_{-a}^{a} \Delta u_x(x)\, dx = (1 - \nu)\sigma_0 a^2 \pi. \tag{A4}$$

(2) *Two asymmetrical colinear cracks*

Let the cracks L_1 and L_2 be located on the segment of the x-axis, $d<x<c$ and $b<x<a$ respectively, with $c<b$. We write (Muskhelishvili 1953, pp. 494–498)

$$\Phi(z)=\Omega(z)=\frac{\sigma_0}{2\pi[R(z)]^{1/2}}\int_{L_1+L_2}\frac{[R(t)^+]^{1/2}}{t-z}\,dt+\frac{pz+q}{2R(z)^{1/2}} \tag{A5}$$

where $R(z)=(z-a)(z-b)(z-c)(z-d)$ and the superscript + (and −) denotes the value(s) of the function on the x-axis from above (and below) respectively. Conditions of single-valuedness of the displacement yield

$$\int_{L_k}(\Phi^+(t)-\Phi^-(t))\,dt=0 \quad (k=1,2). \tag{A6}$$

The conditions (A6) determine the complex constants p and q.

The result of the integration of (A5) is

$$\Phi(z)=\Omega(z)=i\sigma_0/2+(pz+q-i\sigma_0\eta(z))/2(R(z))^{1/2}, \tag{A7}$$

where $\eta(z)=z^2+C_1z+C_2$, $C_1=-(a+b+c+d)/2$ and $8C_2=2(a+b)(c+d)-(a-b^2)-(c-d)^2$. Integration of (A6) yields

$$p=0 \quad \text{and} \tag{A8}$$

$$q=\frac{i\sigma_0}{2}\left(-\frac{(a+b-c-d)^2}{4}+(a-c)(b-d)\frac{E(k)}{K(k)}\right),$$

where $K(k)$ and $E(k)$ are the complete elliptic integrals of the first and second kinds, with $k^2=(a-b)(c-d)/(a-c)(b-d)$.

The stress intensity factors at $x=a$, b, c and d are,

$$\begin{aligned}
K_a&=\sigma_0\left(\frac{\pi(a-c)}{2(a-b)(a-d)}\right)^{1/2}\left(a-d-(b-d)\frac{E(k)}{K(k)}\right),\\
K_b&=\sigma_0\left(\frac{\pi(b-d)}{2(a-b)(b-c)}\right)^{1/2}\left(c-b+(a-c)\frac{E(k)}{K(k)}\right),\\
K_c&=\sigma_0\left(\frac{\pi(a-c)}{2(c-d)(b-c)}\right)^{1/2}\left(c-b+(b-d)\frac{E(k)}{K(k)}\right),\\
K_d&=\sigma_0\left(\frac{\pi(b-d)}{2(c-d)(a-d)}\right)^{1/2}\left(a-d-(a-c)\frac{E(k)}{K(k)}\right).
\end{aligned} \tag{A9}$$

It is sufficient to derive the expression for the moment of one crack; we consider only the left crack. The displacement discontinuity is

$$\Delta u_x(x)=\frac{2\sigma_0(1-\nu)}{\mu}\int_d^x\frac{s^2+C_1s+C_3}{[(s-d)(c-s)(b-s)(a-s)]^{1/2}}\,ds, \tag{A10}$$

where

$$C_3=(-(a-c)(b-d)E(k)/K(k)+ab+cd)/2.$$

Interchanging the order of integration and after some algebraic manipulation, we have

$$\begin{aligned}
M/\sigma_0(1-\nu)&=2\int_d^c(s^2+C_1s+C_3)\left(\frac{c-s}{(s-d)(b-s)(a-s)}\right)^{1/2}ds\\
&=((a-c)/(b-d))^{1/2}((b-c)(a+b-c-d)K(k)\\
&\quad+(b-d)(3c-a-b-d)E(k))/2+\pi((a+b-c-d)^2-4(a-c)(b-d)\\
&\quad\times E(k)/K(k))(1-\Lambda_0(\theta,k))/4,
\end{aligned} \tag{A11}$$

where

$$\Lambda_0(\theta,k)=2(E(k)F(\theta,k')+K(k)E(\theta,k')-K(k)F(\theta,k'))/\pi,$$

$$(k')^2=1-k^2, \qquad \theta=\sin^1((1-\delta^2)^{1/2}/k')$$

$$\delta^2=(c-d)/(b-d)$$

and $F(\theta,k')$ and $E(\theta,k')$ are incomplete elliptic integrals of the first and second kinds.

APPENDIX II

Crack in an infinite periodic array

We assume an infinite periodic array of cracks lies along the x-axis. The k-th crack is assumed to be situated on the segment $2kb - c < x < 2kb + c$, where k is the integer label for the crack. Thus the crack size and spacing are $2c$ and $2b - 2c$, respectively.

Koiter (1959) obtained

$$\Phi(z) = \Omega(z) = \frac{i\sigma_0}{2} - \frac{i\sigma_0}{2} \frac{\sin(\pi z/2b)}{[\sin^2(\pi z/2b) - \sin^2(\pi c/2b)]^{1/2}}.$$

Hence, the stress intensity factor and the displacement discontinuity are written as

$$K = \sigma_0[2b \tan(\pi c/2b)]^{1/2} \tag{A14}$$

and

$$\Delta u_x(x) = \frac{2b}{\pi\mu}(1-\nu)\sigma_0 \log\left[\frac{\cos(\pi x/2b) + (\sin^2(\pi c/2b) - \sin^2(\pi x/2b))^{1/2}}{\cos(\pi c/2b)}\right].$$

The moment is obtained from the numerical integration of $\mu\Delta u_x(x)$ from $x = -c$ to $+c$.